Physics of Fluids

RESEARCH ARTICLE | JUNE 24 2024

Dynamic modeling of a cantilever reed valve considering squeeze flow with experimental validation

Mingming Zhang ; Yuchuan Zhu ; Linfei Li; Jie Ling

Physics of Fluids 36, 067131 (2024)
https://doi.org/10.1063/5.0213400

AIP Publishing

Physics of Fluids ARTICLE pubs.aip.org/aip/pof

Dynamic modeling of a cantilever reed valve considering squeeze flow with experimental validation

Cite as: Phys. Fluids **36**, 067131 (2024); doi: 10.1063/5.0213400
Submitted: 10 April 2024 · Accepted: 5 June 2024 ·
Published Online: 24 June 2024

View Online Export Citation CrossMark

Mingming Zhang, Yuchuan Zhu,[a] Linfei Li, and Jie Ling

AFFILIATIONS

College of Mechanical and Electrical Engineering, Nanjing University of Aeronautics and Astronautics, Nanjing 210016, China

[a]Author to whom correspondence should be addressed: meeyczhu@nuaa.edu.cn

ABSTRACT

Piezoelectric hydraulic pumps play a pivotal role in more electric aircraft and all-electric aircraft utilizing power-by-wire technology, owing to their high power density and reliability. The cantilever reed valve (CRV) serves as a crucial component within these pumps, and its dynamic behavior within the fluid directly impacts the pumps' output power. A precise mathematical model of the CRV is essential for understanding its motion mechanisms. However, existing models for the CRV inadequately capture its dynamics and fail to explain the observed motion phenomena. Further exploration into dynamic modeling of the CRV is warranted. This paper employs finite element analysis to investigate CRV's dynamics, revealing the significant impact of squeeze flow on CRV's dynamics and identifying the cause of slow closure. Based on this, a novel lumped parameter model incorporating squeeze force is proposed to accurately depict CRV's dynamics, particularly focusing on the phenomenon of slow closure. To validate the proposed model's accuracy, an experimental system capable of independently driving the CRV is constructed to eliminate interference resulting from integrating the CRV into the pumps. The results show that the dynamic response during closure, as predicted by the proposed model, is in good agreement with the outcomes from finite element analysis. Notably, the proposed model exhibits an 11.11% higher prediction accuracy for experimental closing times compared to the traditional model that neglects squeeze forces. This study offers guidance for optimizing CRV's dynamics and improving the performance of piezoelectric hydraulic pumps in future applications.

I. INTRODUCTION

Piezoelectric hydraulic pumps are utilized as actuators in power-by-wire technology for advanced more electric and all-electric aircraft[1,2] due to their high power density,[3] precision, and reliability.[4] Increasing the driving frequency[5] is an effective method to enhance the output power of these pumps, although it poses challenges to the dynamic behavior of rectification components.[6] Among these components, the cantilever reed valve (CRV), known for its simple design and efficient shut-off capability,[7] is a common rectification element in piezoelectric hydraulic pumps.[8] However, the CRV exhibits poor dynamic characteristics, which can lead to backflow at high frequency, thereby reducing the flow rate of pumps.[9,10] Consequently, there has been a recent research focus on investigating the key factors influencing the dynamic characteristics of the CRV.

Operating as a passive valve, the motion of the CRV is controlled by the differential pressure acting across its surfaces.[11] Many studies employ a single-degree-of-freedom spring-mass-damping model to analyze the dynamic characteristics of the CRV.[12–15] However, the three parameters used in the model, namely, spring, mass, and damping, are approximately equivalent. It is usually only applicable to a specific working condition and lacks universality. Some research has delved into the impact of fluid on the dynamic attributes of cantilever beams.[16] Naik *et al.* analyzed how liquid properties and gap height affect the resonant response of cantilever beams by considering additional mass and damping coefficients.[17] Lajimi and Heppler used a power series expansion to calculate the natural frequencies of cantilever beams under various parameters.[18] Huang *et al.* performed finite element analysis on the characteristic section of a cantilever beam coated with a piezoelectric macrofiber composite, deriving expressions for the real and imaginary parts of the hydrodynamic function through fitting.[19] Ling *et al.* performed the wet modal analysis of CRVs using ANSYS, revealing that the first-order resonance frequency decreases with increasing fluid pressure.[20]

The dynamic characteristics of cantilever beams immersed in a fluid have been extensively investigated. However, beyond the

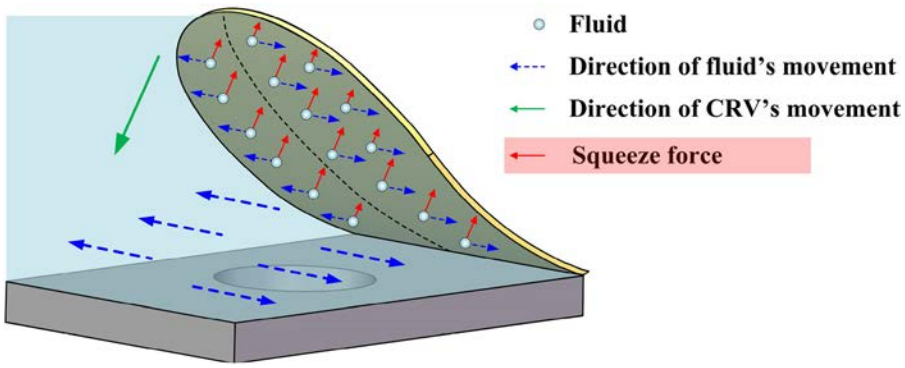

FIG. 1. The diagram of the squeeze flow hindering cantilever reed valve's movement during the closing process.

influence of fluid, the motion of the cantilever reed valve (CRV) is also impacted by the valve cover, which functions to secure the CRV in place. Moimás *et al.* conducted experiments to evaluate the influence of the valve-seat gap on the dynamic behavior of reed-type valves.[21] When the CRV moves closer to the valve cover, it squeezes the fluid between the CRV and the valve cover. The fluid is squeezed to flow radially from the center to the periphery of the CRV, as shown in Fig. 1. Accordingly, the fluid exerts a reactive force on the CRV, known as the squeeze force, hindering the closing motion. However, this squeeze flow phenomenon is presently disregarded in the dynamic modeling of the CRV, making it difficult to accurately describe the motion of the CRV in the fluid. This modeling limitation hinders the identification of critical factors that impede the enhancement of the CRV's dynamic characteristics.

In addition, current experimental systems have limitations when investigating the dynamic characteristics of the CRV. Current experimental techniques involve integrating the CRV into a piezoelectric hydraulic pump for high-frequency excitation and dynamic response observation.[22,23] Wu *et al.* used a laser displacement sensor and a piezoelectric hydraulic pump integrated with a check valve to monitor the dynamic response for the check valve.[24] Dong *et al.* compared wheeled check valves and umbrella valves by analyzing the output flow of the piezoelectric hydraulic pump.[25] He *et al.* investigated the impact of wheel check valve parameters on output pressure using the pump.[26] Nonetheless, these approaches have limitations. The coupling of the CRV and the piezoelectric hydraulic pump introduces potential effects from piezoelectric materials, pump chambers, and pipelines, making the isolated study of the CRV's dynamic characteristics impractical. Given these constraints, it is necessary to develop an experimental system specifically designed to excite the CRVs.

This paper focuses on the dynamic modeling of the CRV during closure. Initially, through finite element analysis, it is characterized that the CRV is subjected to the force of the squeeze flow during the closing process, which can significantly hinder its movement. Subsequently, a novel single-degree-of-freedom lumped parameter model that includes the squeeze force is proposed to accurately model the dynamics of CRV in the closing process. By comparing the outcomes with those of finite element analysis, it is validated that the proposed model can effectively substitute finite element analysis in characterizing the CRV's dynamic traits, addressing issues related to extensive computation and non-convergence in finite element analysis. Furthermore, a dynamic experimental system based on a piezoelectric high-speed on-off valve is constructed to assess the predictive ability of the proposed model under actual working conditions. The experimental system uses a piezoelectric high-speed on-off valve to independently excite the CRV without integrating the CRV into piezoelectric hydraulic pump, minimizing potential external interference.

The novelty of this work is to propose a mathematical model considering squeeze force to describe the impact of squeeze flow on the dynamic behavior of the CRV during closure. The accuracy of the proposed model is verified by finite element analysis and experiments.

II. STRUCTURE OF CANTILEVER REED VALVE

The CRV is fabricated using a wire-cutting process from an elastic metallic material. The non-working region of the CRV is fixed by the valve cover, as illustrated in Fig. 2(a), where the CRV is positioned atop the valve hole represented by the red dotted line. An increase in the differential pressure across the CRV leads to its opening, causing the working region to move away from the valve hole. The working region is opened by the action of oil. The oil exits through this working

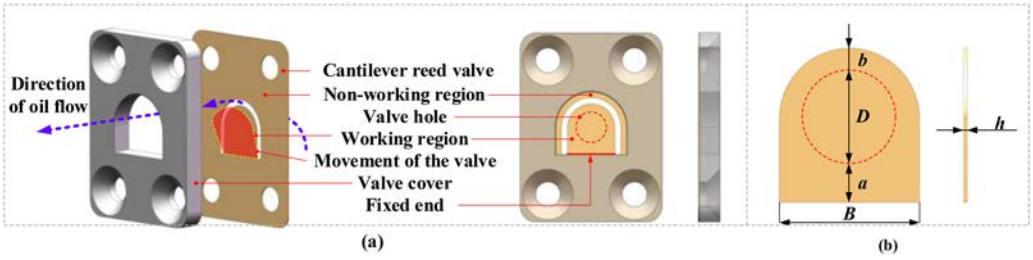

FIG. 2. (a) Assembly of the cantilever reed valve and valve cover and (b) working region of the cantilever reed valve.

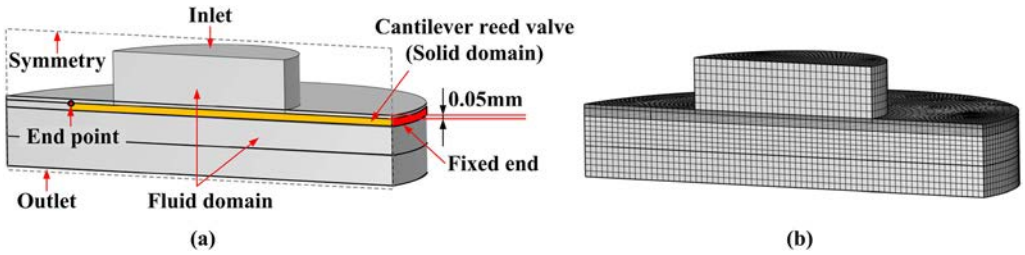

FIG. 3. The finite element model: (a) simplified three-dimensional model and (b) meshed model.

region. Conversely, when the differential pressure decreases, the CRV undergoes a closing motion, resulting in the working region completely attaching the valve hole. The dimensions of the working region are detailed in Fig. 2(b). The CRV's design integrates a combination of semicircular and rectangular elements rather than a simple rectangle to ensure weight minimization. The diameter of the valve hole D corresponds to the area exposed to fluid forces. The dimension a is the distance between the valve hole and the fixed end. The overall width and thickness of the CRV are denoted by "B" and "h," respectively.

III. FINITE ELEMENT ANALYSIS

A. Establishment of finite element model

To study the dynamics of CRV during the closing process, finite element analysis is executed employing the COMSOL software. A finite element model of the CRV is constructed. As illustrated in Fig. 3(a), a simplified three-dimensional model of the CRV and its corresponding fluid domain is developed. The top of the model is designated as the pressure inlet for the fluid, while the bottom serves as the pressure outlet. The CRV forms the solid domain, while all other regions are considered as the fluid domain. To reduce computational workload, symmetry planes are applied to both the solid and fluid domains.

Ideally, the CRV completely separates the fluid domain. However, in the finite element analysis, it is necessary to initialize a continuous fluid domain to ensure smooth simulation. Hence, an initial gap of 0.05 mm is introduced in the finite element model. For displacement measurement, a point probe is placed at the end point of the CRV. The finite element model is meshed using a top-down swept hexahedron structured mesh. The mesh near the CRV is refined using multi-layer mesh refinement to enhance the mesh quality and accommodate dynamic mesh requirements, as depicted in Fig. 3(b). The inlet pressure is set to be a square wave with an amplitude of 20 kPa and a transition time of 1 ms, as shown in Fig. 4. The outlet pressure is set to 0. The CRV is comprised of beryllium bronze (density: 8950 kg/m^3, Young's modulus: 110 GPa), and the fluid used is No. 46 anti-wear hydraulic oil (density: 875 kg/m^3, dynamic viscosity: 0.0484 Pa s).

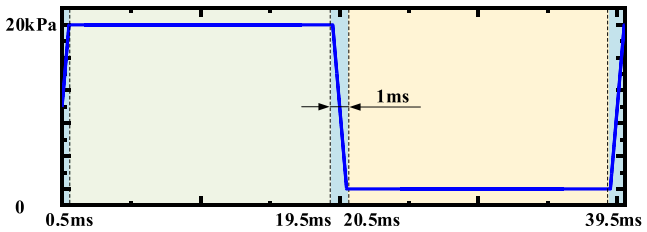

FIG. 4. The curve of inlet pressure.

B. Dynamic response in finite element analysis

Mesh independence verification is conducted to ensure both high precision and optimal utilization of computational resources. The dynamic response of the CRV for different mesh numbers is presented in Fig. 5. It can be observed that the curves are nearly coincident. Key performance parameters adopted for evaluation purposes are enlisted in Table I. The steady-state displacement signifies the displacement of the CRV when it reaches stability. The fall time denotes the time required for the CRV to decrease from 90% to 10% of the steady-state displacement. The closing time represents the time needed for the displacement to reach 2% of the steady-state displacement. Compared with simulations using higher mesh numbers, a mesh number of 42 564 maintains the steady-state displacement error within 0.21%, the falling time error within 2.11%, and the closing time error within 2.32%. Therefore, select the mesh number of 42 564.

It is evident that the dynamic response during the opening and closing processes is asymmetric, with the closing speed notably slower than the opening speed. The closing speed initially increases and then gradually decreases, resulting in an extended closing time. Consequently, a detailed investigation of the closing process is conducted.

C. Analysis of squeeze force

To examine the pressure of the fluid exerted on the CRV during the closing process, a specific surface near the inlet of the CRV is

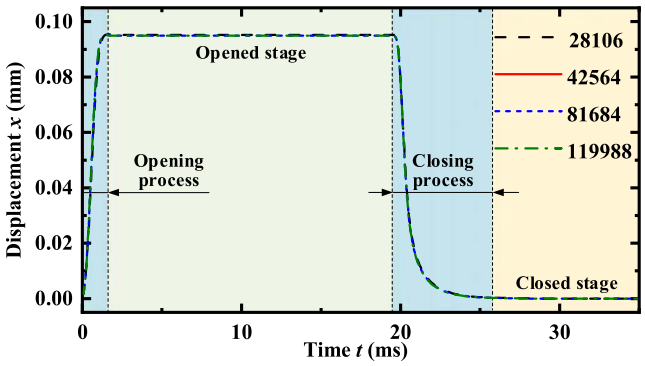

FIG. 5. The dynamic response of CRV under pressure excitation.

TABLE I. The specific evaluation parameters under different mesh numbers.

Mesh number	Steady-state displacement	Fall time	Closing time
28 106	0.0952 mm (0.11%)	1.46 ms (2.82%)	3.74 ms (3.61%)
42 564	0.0951 mm	1.42 ms	3.88 ms
81 684	0.0950 mm (0.11%)	1.40 ms (1.41%)	3.80 ms (2.06%)
119 988	0.0949 mm (0.21%)	1.39 ms (2.11%)	3.79 ms (2.32%)

chosen. This selected surface is illustrated in Fig. 6(a). To observe the squeeze force on different regions of the CRV, the selected surface is divided into three parts, as displayed in Fig. 6(b). Among them, part C faces the inlet. Parts A and B are facing the valve cover. The pressure contours of the surface at various time points are illustrated in Figs. 6(c)–6(h). As observed in Fig. 4, the reduction in inlet pressure commences at 19.5 ms. At this point, the primary resistance faced by the CRV stems from the pressure exerted on part C. At 20 ms, as depicted in Fig. 4, the inlet pressure has decreased to 10 kPa, aligning closely with the pressure on part C. However, unlike at 19.5 ms, the pressure on part A surpasses that on part C and becomes the primary resistance to the CRV's closure. At 20.5 ms, the inlet pressure descends to 0 kPa, with the pressure on part C concurrently dropping to 0 kPa, while the pressure on part A remains the highest among the three parts. As the CRV progresses in closure, the pressures on parts A and B decrease progressively. By 21 ms, the pressure on part B equals that of part A. Subsequently, beyond 21 ms, the pressure on part B surpasses that on part A.

In order to mitigate fluid resistance to the CRV, the distance between the CRV and the valve cover is increased. Figure 7 illustrates the pressure contours when the initial distance between the CRV and the valve cover is 0.20 mm. At 19.5 ms, the pressure contour resembles that of the initial 0.05 mm distance, with the predominance of pressure at part C. As the CRV continues to close, the pressure at part C remains the primary source of resistance. At 20.5 ms, the inlet pressure decreases to 0 kPa, concurrently reducing the pressure on the CRV to 0 kPa. Throughout the closure process, the pressures on parts A and B consistently remain lower than that on part C.

It is evident that the distance between the CRV and the valve cover (0.05 mm) results in fluid resistance during CRV closure, while this resistance is absent with a larger distance (0.20 mm). In practice, this distance should be very small due to the cutoff of CRV. As the

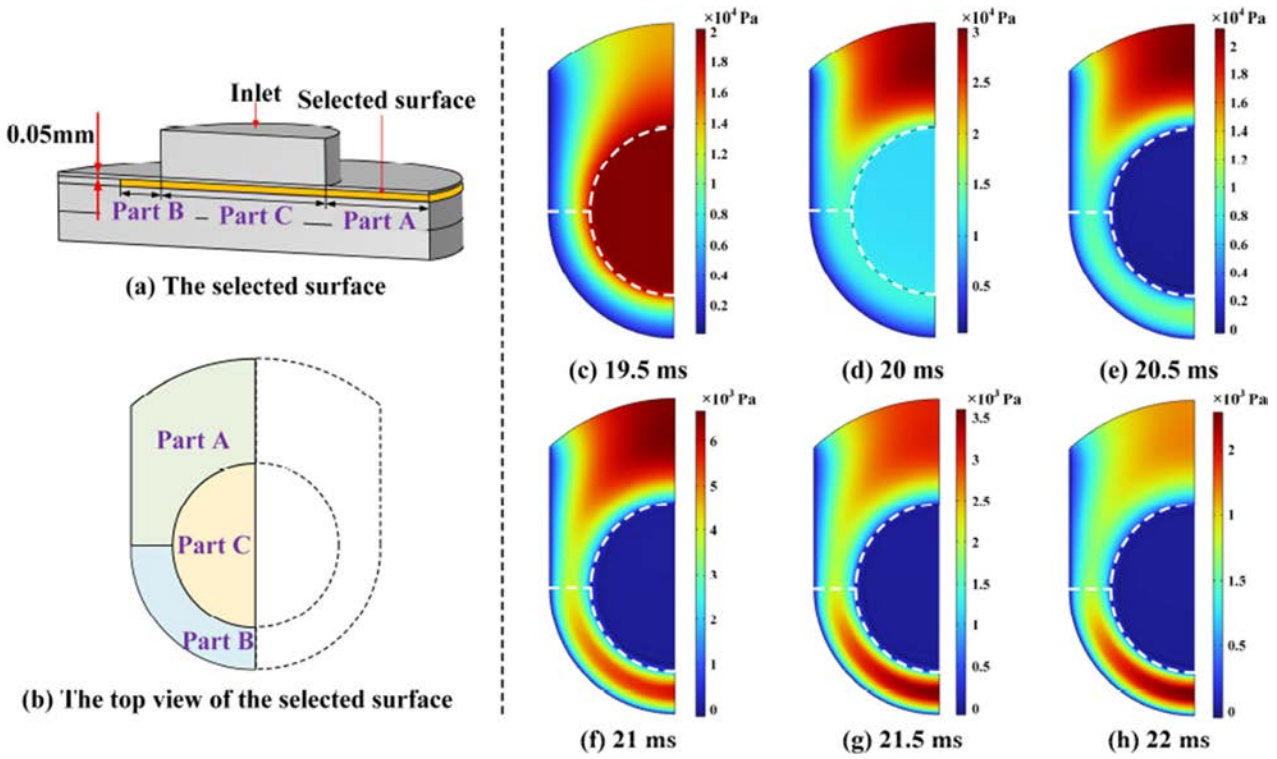

FIG. 6. (a) The schematic diagram of the selected surface; (b) the top view of the selected surface; and (c)–(h) the pressure contours when the initial distance between the CRV and the valve cover is 0.05 mm.

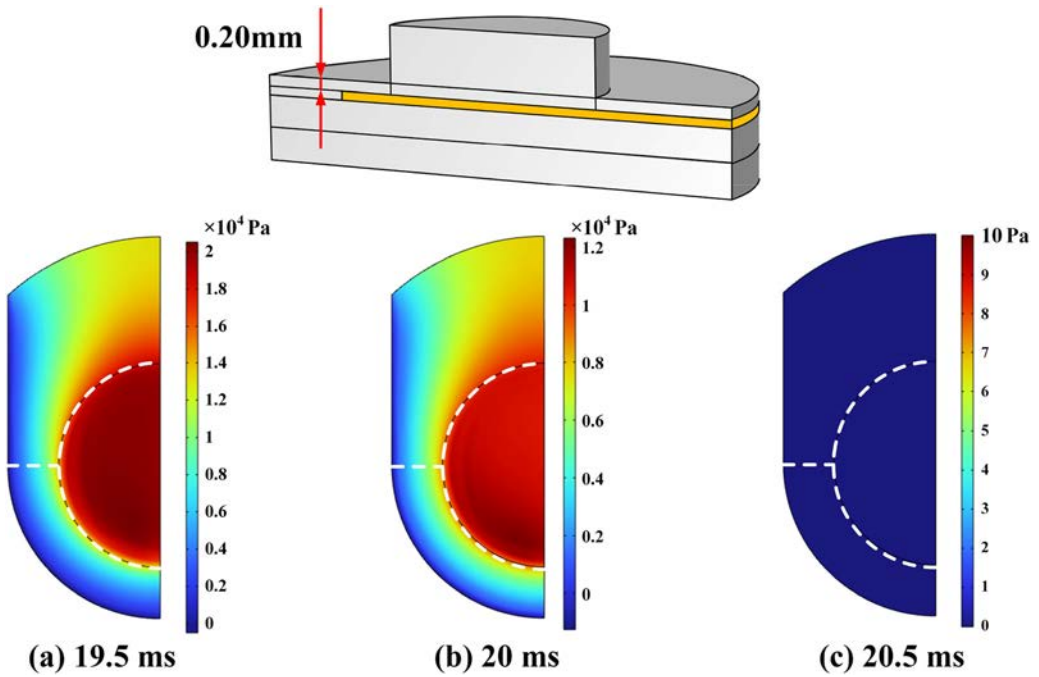

FIG. 7. The pressure contours when the initial distance between the CRV and the valve cover is 0.20 mm.

CRV closes, it gradually approaches the valve cover, exerting a squeezing effect on the fluid in the gap. In response, the fluid generates a reaction force on the CRV, hindering its closing motion. The fluid resistance encountered by the CRV during closure is referred to as the squeeze force.

The squeeze force arises from the relative motion between the CRV and the valve cover. Modifying this distance results in a change in the squeeze force. Therefore, an initial distance ranging from 0.05 to 0.30 mm between the CRV and the valve cover is selected to investigate the influence of the squeeze force on the CRV's dynamic response during closure. The displacement of the end point marked in Fig. 3 is extracted and regarded as the displacement of the CRV, which is represented by a red line in Fig. 8. It is noted that as the initial distance increases, the dynamic response of the CRV during closure accelerates. At an initial distance of 0.15 mm, displacement overshoot is observed. This phenomenon occurs because the widening initial distance reduces the CRV's squeezing effect on the fluid, resulting in a decrease in CRV's resistance.

When the initial distance is 0.05 mm, there is a peak on the force curve of part A, which is caused by the strong squeezing effect. As the initial distance increases, the squeezing effect gradually weakens, resulting in a gradual decrease in the force on part A.

The pressure on parts A, B, and C is integrated to determine the resistance of each part, as illustrated in Fig. 8. The resistance of part C is represented by the blue line, while the resistances of parts A and B are represented by a black line and green line, respectively. It becomes clear that the resistance of part C is independent of the initial distance, relying solely on the inlet pressure. At an initial distance of 0.05 mm, part A surpasses part C in resistance after 19.7 ms, becoming the dominant resistance in the CRV. Subsequently, after 20.15 ms, the resistance of part B also exceeds that of part C. Thus, at an initial distance of 0.05 mm, the fluid's squeeze force significantly impacts the closing motion of the CRV. As the initial distance increases, the squeeze force exerted by the fluid on the CRV gradually diminishes, weakening its influence on the closing motion. At an initial distance of 0.2 mm, the resistance of part C consistently exceeds that of parts A and B due to the reduced squeeze force. Consequently, the CRV's resistance during closure decreases, leading to displacement overshoot, as indicated in Fig. 8(d). Moreover, the figure illustrates that part A exhibits higher resistance, acting as the primary hindrance to the closing motion. Therefore, reducing the size of part A in the structural design can enhance the dynamic response.

IV. MATHEMATICAL MODEL OF CANTILEVER REED VALVE

The squeeze force is considered in the mathematical modeling to accurately describe the dynamics of the CRV during the closing process.

A. Deflection curve equation

The CRV functions as a cantilever beam with one end fixed and the other free. When subjected to fluid pressure, the CRV bends, resulting in an output displacement, as depicted in Fig. 9(a). Assuming a uniformly distributed fluid pressure p acting on the CRV and approximating its shape to that of a rectangular structure, the schematic is presented in Fig. 9(b).

During the bending of the cantilever beam, the deflection and rotational angle of each point on the beam vary according to their positions. The beam is segmented into three regions: regions I, II,

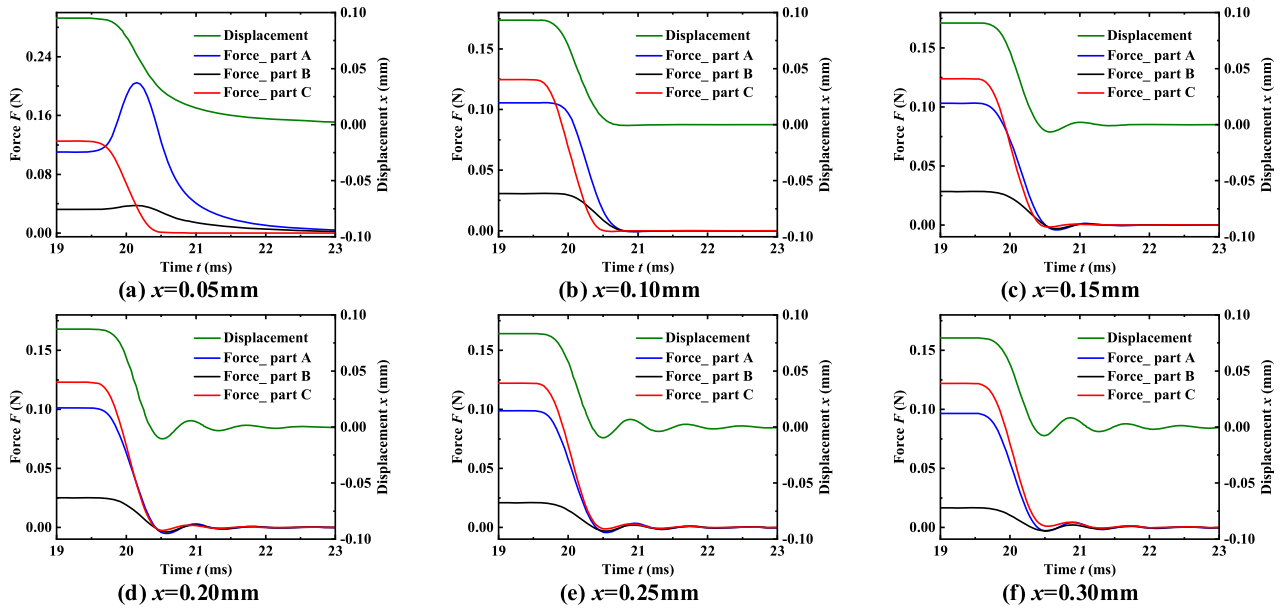

FIG. 8. The displacement and resistance of CRV at different initial distances.

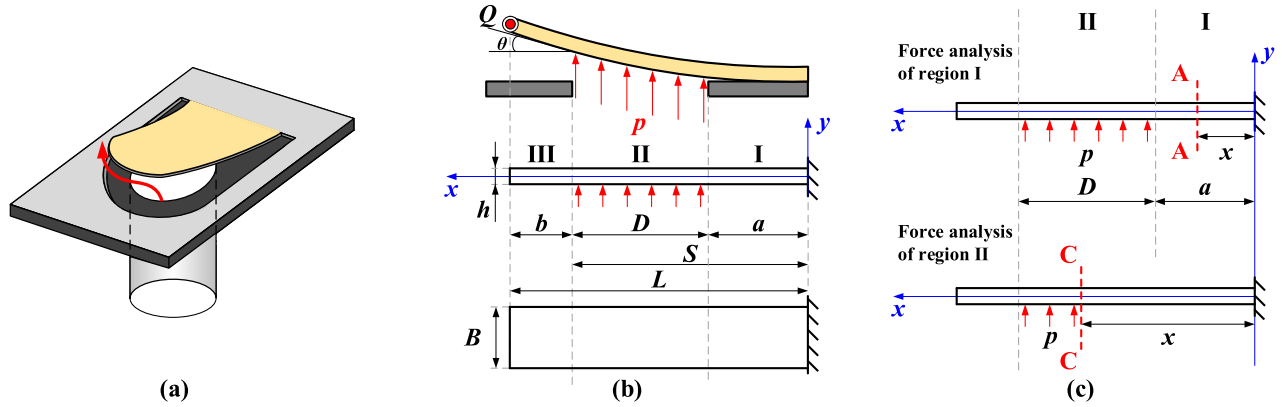

FIG. 9. (a) The working schematic of the cantilever reed valve, (b) the structure of the cantilever reed valve, and (c) the force analysis diagram of the cross section on regions I and II.

and III. Select the cross section A–A on the region I, as shown in Fig. 9(c). The force analysis of its left part is carried out, and the shear force $F_s(x)$ and bending moment $M(x)$ are

$$\begin{cases} F_s(x) = pBD, \\ M(x) = pBD\left(\dfrac{D}{2} + a - x\right), \end{cases} \quad 0 \le x < a, \tag{1}$$

where pB is the surface-uniform loading of the cantilever beam. For CRV, the surface-uniform loading per unit area is the product of pressure p and width B.

Select the cross section C–C on the region II, as shown in Fig. 9(c). The force analysis of its left part is carried out, and the shear force and bending moment are

$$\begin{cases} F_s(x) = pB(D + a - x), \\ M(x) = pB\dfrac{(D + a - x)^2}{2}, \end{cases} \quad a \le x < S. \tag{2}$$

Because the left part of any section in region III is not subjected to force, the shear force and bending moment of any section in region III are

$$\begin{cases} F_s(x) = 0, \\ M(x) = 0, \end{cases} \quad S \le x < L. \tag{3}$$

In the case of pure bending, the relationship between the bending moment and curvature ρ is

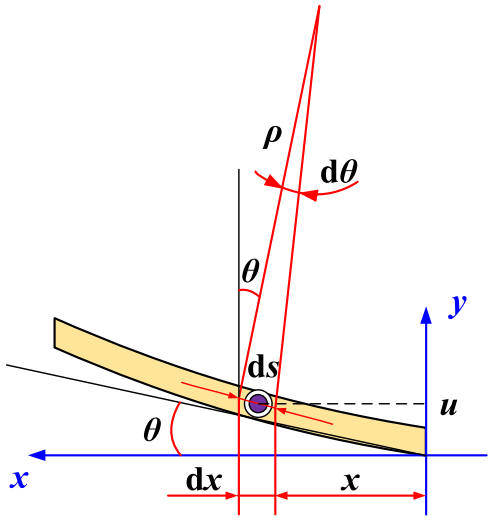

FIG. 10. The bending diagram of the cantilever beam.

$$\frac{1}{\rho}=\frac{M}{EI}, \tag{4}$$

where M and ρ are functions of x, E is the elastic modulus of the valve material, and I is the cantilever beam's sectional moment of inertia. For the rectangular section, $I=Bh^3/12$.

From Fig. 10, when the beam is bent, the deflection u of the cross section at the position x and its rotation angle θ relative to the axis x can be expressed as

$$\tan\theta=\frac{\mathrm{d}u}{\mathrm{d}x}. \tag{5}$$

The curvature ρ can be expressed as

$$\mathrm{d}s=\rho\mathrm{d}\theta, \tag{6}$$

where $\mathrm{d}s$ is the arc length of the differential segment. The combined formulas (5) and (6) can be obtained:

$$\frac{1}{\rho}=\frac{\mathrm{d}\theta}{\mathrm{d}s}=\frac{\mathrm{d}\theta}{\mathrm{d}x}\frac{\mathrm{d}x}{\mathrm{d}s}=\frac{\mathrm{d}}{\mathrm{d}x}\left[\arctan\left(\frac{\mathrm{d}u}{\mathrm{d}x}\right)\right]\frac{\mathrm{d}x}{\mathrm{d}s}=\frac{\dfrac{\mathrm{d}^2u}{\mathrm{d}x^2}}{1+\left(\dfrac{\mathrm{d}u}{\mathrm{d}x}\right)^2}\frac{\mathrm{d}x}{\mathrm{d}s}. \tag{7}$$

In addition, it is noted from Fig. 9(c) that

$$\frac{\mathrm{d}x}{\mathrm{d}s}=\cos\theta=(1+\tan^2\theta)^{-\frac{1}{2}}. \tag{8}$$

Substituting formulas (7) and (8) into formula (4), we obtain

$$\frac{M}{EI}=\frac{1}{\rho}=\frac{\dfrac{\mathrm{d}^2u}{\mathrm{d}x^2}}{\left(1+\left(\dfrac{\mathrm{d}u}{\mathrm{d}x}\right)^2\right)^{\frac{3}{2}}}. \tag{9}$$

Since the value of $\mathrm{d}u/\mathrm{d}x$ is very small, $(\mathrm{d}u/\mathrm{d}x)^2$ in formula (9) can be omitted compared with 1. Therefore, the approximate differential equation of the deflection curve can be obtained as

$$\frac{M}{EI}=\frac{\mathrm{d}^2u}{\mathrm{d}x^2}. \tag{10}$$

The substitution of formulas (1) and (2) into formula (10) yields the deflection curves of the I and II sections, which are obtained by the boundary condition of $u=0$, $\dot{u}=0$ at $x=0$,

$$u(x)=\begin{cases}\dfrac{pBD(3ax^2+3Sx^2-2x^3)}{12EI}, & 0\le x\le a,\\ \dfrac{pB(x^4-4Sx^3+6S^2x^2-4a^3x+a^4)}{24EI}, & a<x\le S.\end{cases} \tag{11}$$

The rotation angle formula of the II section is

$$\theta(x)=\frac{pB(x^3-3Sx^2+3S^2x-a^3)}{6EI}, \quad a<x\le S. \tag{12}$$

The deflection curve of the III section is

$$u(x)=(x-S)\theta(S)+u(S)=\frac{pB(4S^3x-4a^3x+a^4-S^4)}{24EI}, \quad S<x\le L. \tag{13}$$

The displacement of the cantilever beam's end Q is expressed as $u(L)$. Consequently, the displacements of the remaining points along the beam can be expressed as

$$u(x)=\begin{cases}\dfrac{2(S-a)(3ax^2+3Sx^2-2x^3)}{3S^4+4bS^3-4a^3S-4a^3b+a^4}u(L), & 0\le x\le a,\\ \dfrac{x^4-4Sx^3+6S^2x^2-4a^3x+a^4}{3S^4+4bS^3-4a^3S-4a^3b+a^4}u(L), & a<x\le S,\\ \dfrac{4S^3x-4a^3x+a^4-S^4}{3S^4+4bS^3-4a^3S-4a^3b+a^4}u(L), & S<x\le L.\end{cases} \tag{14}$$

B. Dynamic model

Since the operational frequency is much smaller than the resonant frequency, the dynamic model of the CRV can be simplified to a lumped parameter model.[27,28] Consequently, the cantilever beam is simplified as a single-degree-of-freedom mass-spring-damping system, with mass concentrated at its end,[29] denoted as point Q in Fig. 11. Owing to the asymmetry in dynamic responses during the opening and closing processes, separate dynamic models are developed for each process:

$$m_e\ddot{u}+c\dot{u}+ku=\begin{cases}F_p-F_h, & \dot{u}\ge 0,\\ F_p-F_h-F_s, & \dot{u}<0,\end{cases} \tag{15}$$

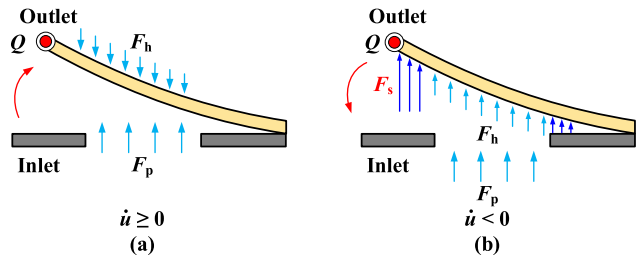

FIG. 11. The force analysis diagram of the cantilever reed valve: (a) opening process and (b) closing process.

where m_e, c, and k are the equivalent mass, damping, and equivalent stiffness of the CRV respectively. F_p is the driving force, which is determined by the differential pressure across the CRV, and F_h represents the combined effect of inertia and viscous forces exerted by the fluid on the CRV during its motion, commonly known as hydrodynamic loading. F_s is the reaction force applied to CRV when the fluid between the CRV and valve cover is squeezed.

1. Equivalent mass m_e

The CRV is simplified as a single-degree-of-freedom mass-spring-damping system with mass concentrated at its end.[30] Throughout this simplification, the kinetic energy T remains constant. Therefore, from the law of conservation of kinetic energy,

$$T = \sum_{i=1}^{N} E_{ki} = \int_0^L \frac{1}{2}\rho Bh[\dot{u}(x)]^2 \mathrm{d}x = \frac{1}{2} m_e [\dot{u}(L)]^2, \tag{16}$$

where ρ is the density of the valve material. The deflection at each point on the CRV is determined using formula (14). Subsequently, the velocity at each point is derived and substituted into formula (16). The equivalent mass is then calculated accordingly,

$$m_e = \rho Bh \left(\begin{aligned} &\int_0^a \frac{2(S-a)(3ax^2+3Sx^2-2x^3)}{3S^4+4bS^3-4a^3S-4a^3b+a^4} \\ &+\int_a^S \frac{x^4-4Sx^3+6S^2x^2-4a^3x+a^4}{3S^4+4bS^3-4a^3S-4a^3b+a^4} \\ &+\int_S^L \frac{4S^3x-4a^3x+a^4-S^4}{3S^4+4bS^3-4a^3S-4a^3b+a^4} \end{aligned} \right). \tag{17}$$

2. Damping c

The damping of the CRV in the air is smaller than that in the fluid, so the damping c in the air is ignored in this modeling. The damping in the fluid is shown in Subsection IV B 5.

3. Equivalent stiffness k

By utilizing formula (13), the deflection of the endpoint Q under pressure p can be obtained, and the equivalent stiffness k can be calculated as follows:

$$k = k_a \frac{pBD}{u(L)} = k_a \frac{24EID}{3S^4+4bS^3-4a^3S-4a^3b+a^4}. \tag{18}$$

The coefficient k_a is considered to account for the fact that the CRV has an arc shape. The sectional moment of inertia is lower than that of the rectangular CRV.

4. Driving force F_p

The driving force F_p is determined by the inlet pressure p_{in} and back pressure p_{out} of the CRV, which can be expressed as

$$F_p = (p_{in}R(t) - p_{out})A, \tag{19}$$

where A is the action area of fluid on the CRV, and $R(t)$ represents the rate at which the inlet pressure changes, taking into account the time necessary for the pressure to stabilize and dissipate, as shown in Fig. 4,

$$R(t) = \begin{cases} 1/2 + t/t_d, & 0 < t < t_d/2, \\ 1, & t_d/2 < t < T/2 - t_d/2, \\ 1 - (t - T/2 + t_d/2)/t_d, & T/2 - t_d/2 < t < T/2 + t_d/2, \\ 0, & T/2 + t_d/2 < t < T - t_d/2, \\ (t - T + t_d/2)/t_d, & T - t_d/2 < t < T, \end{cases} \tag{20}$$

where t_d is the transient time when the inlet pressure is a square wave.

5. Hydrodynamic loading F_h (Additional mass and additional damping)

As the CRV moves within the fluid, the surrounding fluid also follows its motion. Previous researchers regarded this hydrodynamic loading as a contribution to the additional mass and additional damping of the cantilever beam.[31] Also, Sader gave a concise hydrodynamic loading formula for a cantilever beam per unit length:[32]

$$F_h = \frac{\pi}{4}\rho_f \omega^2 B^2 \Gamma u(t), \tag{21}$$

where ρ_f is the fluid density, and ω is the circular frequency of the CRV. Γ is a dimensionless hydrodynamic function, $\Gamma = \Gamma_r + j\Gamma_i$. Then, formula (21) can be expressed as

$$\begin{aligned} F_h &= \frac{\pi}{4}\rho_f \omega^2 B^2 \Gamma_r u(t) + j\frac{\pi}{4}\rho_f \omega^2 B^2 \Gamma_i u(t) \\ &= \frac{\pi}{4}\rho_f B^2 \Gamma_r \frac{\mathrm{d}^2}{\mathrm{d}t^2}u(t) + \frac{\pi}{4}\rho_f \omega B^2 \Gamma_i \frac{\mathrm{d}}{\mathrm{d}t}u(t). \end{aligned} \tag{22}$$

It can be obtained from the formula that the additional mass $m_a = \pi\rho_f B^2 \Gamma_r/4$, and the additional damping $c_a = \pi\rho_f \omega B^2 \Gamma_i/4$. Maali proposed a simplified calculation formula for the hydrodynamic function Γ of a rectangular cantilever beam within the Reynolds number R_e of 0.1–1000:[33]

$$\begin{cases} \Gamma_r = a_1 + \dfrac{a_2}{\sqrt{\mathrm{Re}}}, \\ \Gamma_i = \dfrac{b_1}{\sqrt{\mathrm{Re}}} + \dfrac{b_2}{\mathrm{Re}}, \end{cases} \tag{23}$$

where $a_1 = 1.0553$, $a_2 = 3.7997$, $b_1 = 3.8018$, and $b_2 = 2.7364$.

6. Squeeze force F_s

During the closing process, the CRV moves toward the valve cover, squeezing the fluid between the CRV and valve cover. Due to the relative motion between the CRV and the valve cover, the fluid flows radially from the center of the CRV to the periphery. Accordingly, the fluid exerts a reaction force F_s on the CRV due to the squeezing effect. The fluid flow within the gap between the CRV and valve cover can be approximated as a flow between parallel disks. The velocity of the CRV can be approximated as the velocity of the end point $\dot{u}(L)$. The pressure acting on the CRV is determined by the theory of squeezing flow between parallel disks:

$$dp = \frac{12\mu\dot{u}(L)}{u(L)^3} y dy. \tag{24}$$

Integrate the above equation and the boundary condition is $p = 0$ at $y = B/2$. The pressure distribution law along the single side of the CRV is as follows:

$$p = \frac{6\mu\dot{u}(L)}{u(L)^3}(B^2/4 - y^2). \tag{25}$$

The pressure distribution along the opposite side of the centerline exhibits complete symmetry with respect to this side. The total force F_s acting on the entire CRV is given by

$$F_s = 2k_s \int_0^{B/2} pL dy = \frac{8k_s\mu LB^3\dot{u}(L)}{u(L)^3}. \tag{26}$$

The coefficient k_s considers the fact that the shape of the CRV is not a perfect rectangle and the occurrence of fluid exiting through the valve hole without being extruded.

Formula (26) demonstrates that the squeeze force is dependent on the displacement and velocity of the CRV. This relationship further clarifies the outcomes of the finite element simulations in Sec. III, where the pressure on part A exceeds that on part B due to the closer distance of part A to the valve cover.

V. MODEL VERIFICATION

To validate the proposed model's accuracy, the results derived from the mathematical model are compared with those from finite element analysis and experiments, respectively.

A. Model verification by finite element analysis

The proposed model is built in MATLAB/Simulink, employing the same operating conditions with that of the finite element analysis. Furthermore, the traditional lumped parameter model without considering the squeeze force F_s is added as a control group.[20] Referencing formulas (15), the traditional model can be mathematically represented as follows:

$$m_e\ddot{u} + c\dot{u} + ku = F_p - F_h. \tag{27}$$

All parameters in the traditional model remain consistent with those in the proposed model. This approach is taken to specifically scrutinize the impact that the squeeze force F_s can have on the model's precision. The specific parameters associated with these models are listed in Table II.

The inlet pressure is a square wave. It ranges from 5 to 40 kPa in increments of 5 kPa. The outlet pressure is set to 0. The CRV is subjected to an initial opening impulse at $t = 0$ s, followed by a closure impulse at $t = 20$ ms. The simulation outcomes at the inlet pressures of 10, 20, and 30 kPa are depicted in Fig. 12. The simulation results obtained from the finite element analysis (red dotted line) and the proposed model (black line) closely coincide during the closing process. Conversely, the displacement curve of the traditional model (green line) significantly deviates from the results of finite element analysis in the closing process.

TABLE II. Parameters involved in the models.

Name	Unit	Value	Name	Unit	Value	Name	Unit	Value
a	mm	2.5	A	mm^2	12.56	ρ	kg/m^3	8950
b	mm	1.0	k_a	⋯	0.91	ρ_f	kg/m^3	875
D	mm	4.0	k_s	⋯	0.008	E	Pa	110×10^9
B	mm	6.0	h	mm	0.15	μ	Pa s	0.0484

The fall time denotes the time required for the CRV to decrease from 90% to 10% of the steady-state displacement, with the steady-state displacement representing the stable position when the CRV is open. The closing time represents the time needed for the displacement to reach 2% of the steady-state displacement. Figure 12 shows the capability of the proposed model that can predict the steady-state displacements. Tables III and IV present evaluation parameters for various inlet pressures. With increasing inlet pressure, there is a consistent decrease in the fall time and closing time as projected by the finite element analysis. This trend illustrates an augmented dynamic behavior of the CRV. The proposed model provides successful predictions for fall time and closing time under various inlet pressures. The prediction errors are within 18.86% and 23.85%, respectively. Conversely, the traditional model delivers constant predictions for fall time (0.63 ms) and closing time (1.02 ms), irrespective of the inlet pressure variability, displaying maximum errors of 73.26% and 79.29%. Consequently, under the same working conditions, the proposed model improves the prediction accuracy of the fall time and the closing time by 61.45% and 68.83% in maximum, respectively. This improvement underscores the model's precision after considering the squeeze force.

Upon comparison, it is evident that the dynamic response curve of the CRV, as projected by the proposed model, is in good agreement with the outcomes of finite element analysis. Consequently, the proposed model can serve as a substitute for finite element analysis in describing the dynamic characteristics of the CRV. Notably, actual operational conditions are more complex. Directly integrating actual pressure curves into the finite element model may lead to extensive computations or even convergence issues, particularly concerning the CRV's three-dimensional structure. The proposed model offers a resolution to this challenge. The pressure curves from real operational settings can be substituted into the proposed model to obtain the dynamic response of the CRV quickly and accurately.

B. Model verification by experiments

To investigate the dynamic properties of the CRV under varying operational conditions and confirm the accuracy of the proposed model, a dedicated experimental system has been constructed.

1. The experimental system

An experimental system based on a piezoelectric high-speed on-off valve (PHSV) is developed, as illustrated in Fig. 13. The CRV is excited by the PHSV rather than being integrated into a piezoelectric hydraulic pump. The experimental system consists of a hydraulic power supply, a real-time simulator (Beijing Lingsi Chuangqi Technology Co., Links-Box-03), a CRV fixture, a CRV to be tested, a PHSV, a power amplifier (AE Techron Inc, 7224), two throttle valves (Wuxi Xinli, KC-03), and three high-frequency pressure sensors (Kunshan Shuangqiao, CYG1401F). The high-frequency pressure

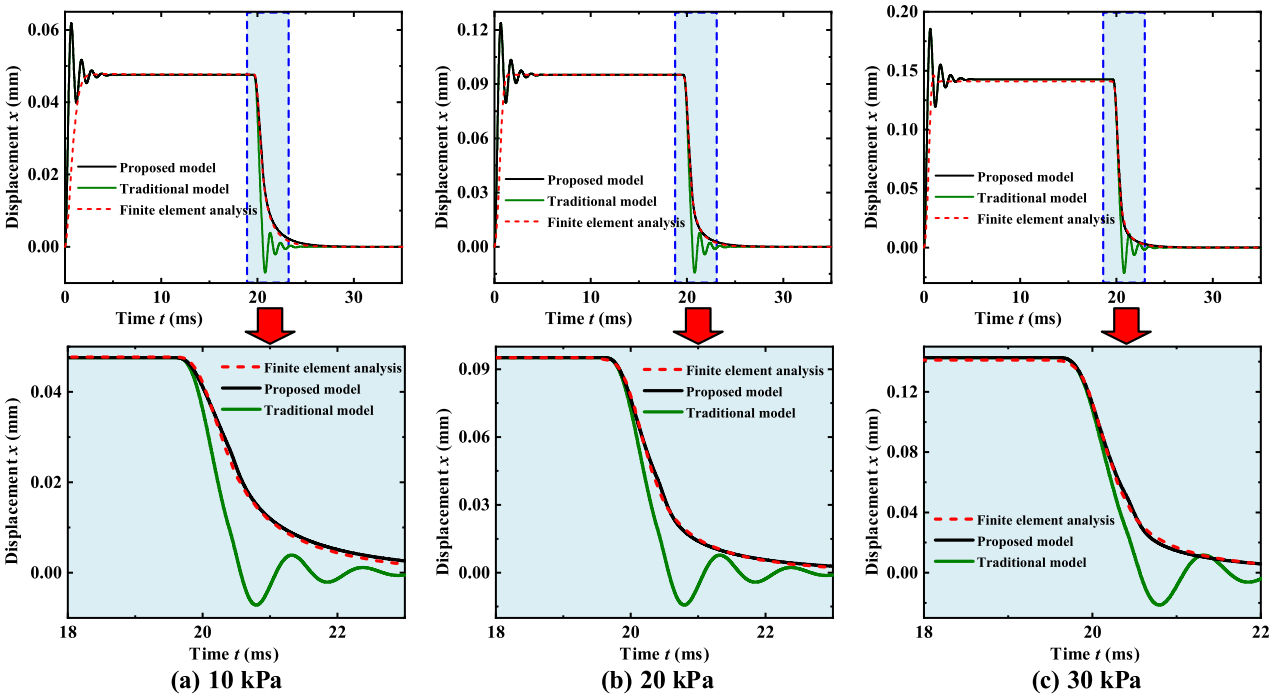

FIG. 12. Comparison of the results from the proposed model, traditional model, and finite element analysis.

TABLE III. Fall time of the proposed model, traditional model, and finite element analysis. The boldface is the condition in which the proposed model has the highest improvement in prediction accuracy compared with the traditional model.

Inlet pressure (kPa)	Finite element analysis (ms)	Proposed model	Traditional model
5	**2.36**	**2.81 ms (18.86%)**	**0.63 ms (73.26%)**
10	1.99	2.16 ms (8.29%)	0.63 ms (68.29%)
15	1.72	1.75 ms (1.86%)	0.63 ms (63.31%)
20	1.42	1.48 ms (4.01%)	0.63 ms (55.56%)
25	1.35	1.28 ms (5.19%)	0.63 ms (53.26%)
30	1.17	1.13 ms (3.33%)	0.63 ms (46.07%)
35	1.15	1.02 ms (11.57%)	0.63 ms (45.13%)
40	1.07	0.93 ms (13.46%)	0.63 ms (41.03%)

TABLE IV. Closing time of the proposed model, traditional model, and finite element analysis. The boldface is the condition in which the proposed model has the highest improvement in prediction accuracy compared with the traditional model.

Inlet pressure (kPa)	Finite element analysis (ms)	Proposed model	Traditional model
5	**4.91**	**6.08 ms (23.85%)**	**1.02 ms (79.29%)**
10	4.40	5.00 ms (13.64%)	1.02 ms (76.89%)
15	4.13	4.58 ms (10.85%)	1.02 ms (75.38%)
20	3.88	4.15 ms (6.83%)	1.02 ms (73.79%)
25	3.56	3.81 ms (6.94%)	1.02 ms (71.43%)
30	3.42	3.53 ms (3.30%)	1.02 ms (70.26%)
35	3.32	3.30 ms (0.54%)	1.02 ms (69.37%)
40	3.17	3.10 ms (2.08%)	1.02 ms (67.92%)

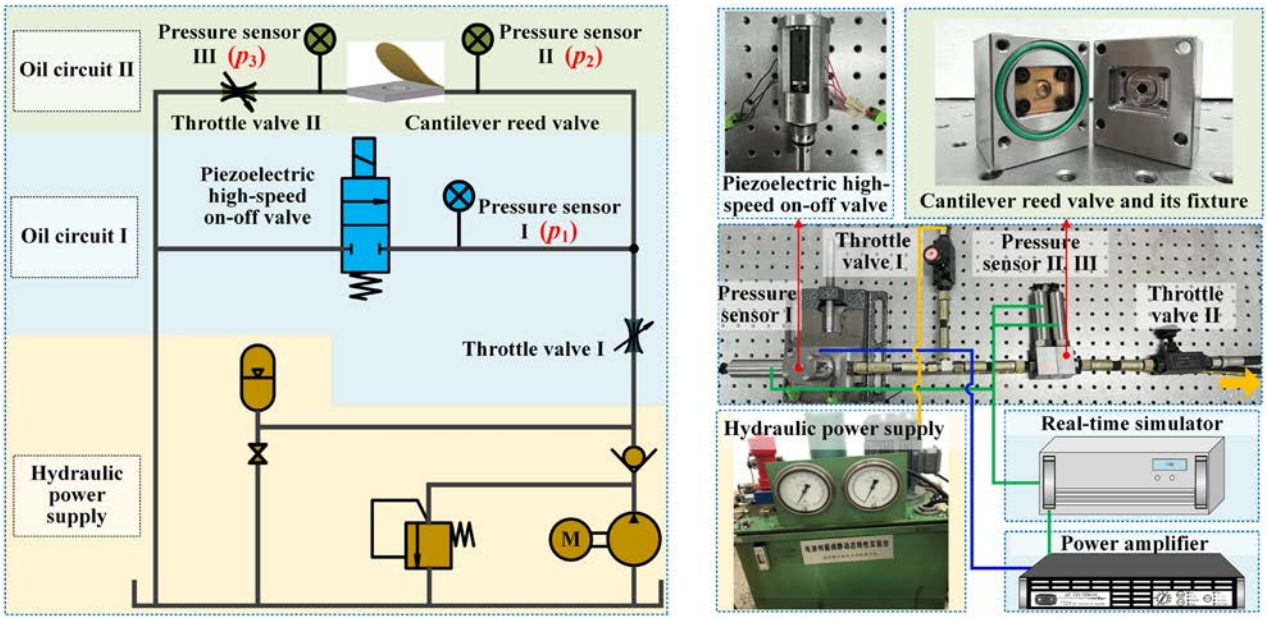

FIG. 13. The hydraulic system diagram and composition of the experimental system.

sensors exhibit a test accuracy of 0.25% full scale and possess a natural frequency of 320 kHz. The prototype of the CRV and its fixture are designed and manufactured, as shown in Fig. 13(b). The PHSV operates as a two-position, two-way valve, generating a square wave pressure excitation for the system that assures rapid pressure establishment and release. This process is powered by the aforementioned power amplifier. The joint employment of the hydraulic power supply and throttle valve I provides a constant current source for the experimental system to match the flow capacity of the PHSV. To actualize the back pressure of the CRV, the aperture of throttle valve II is modulated. The high-frequency pressure sensors I, II, and III are utilized to monitor the inlet pressure of the PHSV p_1, CRV's inlet pressure p_2, and back pressure p_3, respectively.

The following are the detailed steps of the experimental operations:

(a) Initiate the hydraulic power supply and regulate its output pressure to 1.4 MPa. Adjust throttle valve I to control the inlet pressure of the PHSV and CRV.
(b) Transmit a square wave signal, featuring a frequency of 1 Hz and an amplitude of 6.25 V, to the power amplifier via a real-time simulator. The power amplifier amplifies the signal by a factor of 16, resulting in a driving signal for the PHSV of a square wave, with a frequency of 1 Hz and an amplitude of 100 V.
(c) Upon receipt of the square wave signal, the PHSV executes cyclic opening and closing actions. Owing to hydraulic influences, the CRV similarly performs cyclic opening and closing actions, leading to periodic changes in the pressure readings at pressure sensors II and III. The readings from pressure sensors II and III are duly recorded.
(d) Cease the transmission of the square wave signal via the real-time simulator and close the hydraulic power supply.

During each test, the PHSV operates through a minimum of three cycles, facilitating the collection of multiple sets of pressure data and thereby enhancing the reliability of the experimental results.

2. Experimental analysis

The experimental results are depicted in Fig. 14. The pressure p_2 is represented by the orange curve, p_3 by the green curve, and the control signal is denoted by a red dotted curve. The pressure p_d is the difference between p_2 and p_3. When the control signal is 0, the PHSV is closed, and the oil circuit I is disconnected. At this stage, the CRV opens, resulting in a pressure drop between p_2 and p_3. At 500 ms, the control signal increases from 0 to 1. The PHSV transitions into an open state, instigating oil flow via oil circuit I. This causes the oil circuit II to be sucked out. The pressure p_2 and p_3 on the oil circuit II begins to decrease. Then, the CRV does the closing motion. This corresponds to stage I in Fig. 14(b). Upon the CRV fully closing, oil circuit II becomes obstructed, and the pressure p_3 stops falling. This process corresponds to stage II in Fig. 14(b). Accordingly, the termination of p_3's descending trend can be employed as a determinative measure to pinpoint the exact closing time of the CRV. In Fig. 14(b), the inflection point of pressure p_3 is marked by point A, which indicates the moment of complete CRV closure. According to the figure, the closing time of the CRV is 3.4 ms under this condition. During stage III, as depicted in Fig. 14(b), the gradual decrease in pressure p_3 due to leakage eventually falls below pressure p_2, resulting in the reopening of the CRV.

To avoid the potential interference from the pump chamber and piping of the piezoelectric hydraulic pump on test outcomes, the methodology involving the direct excitation of the CRV by the PHSV and the direct measurement of the CRV's inlet and outlet pressures is employed to assess the CRV's dynamic performance.

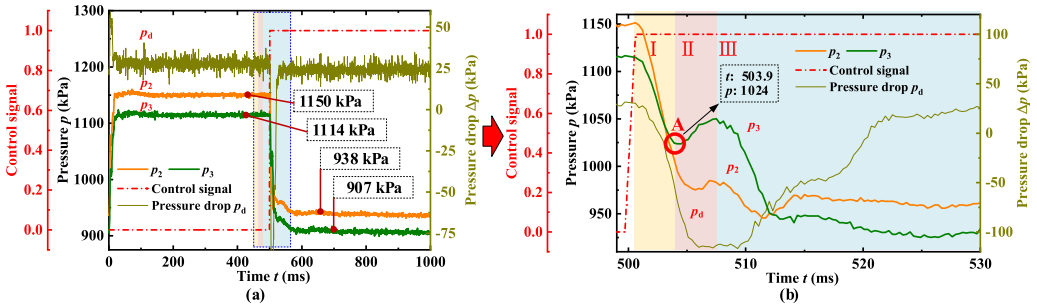

FIG. 14. The experimental results under the first operational condition: (a) curves in one cycle and (b) partial magnified view of the closing process.

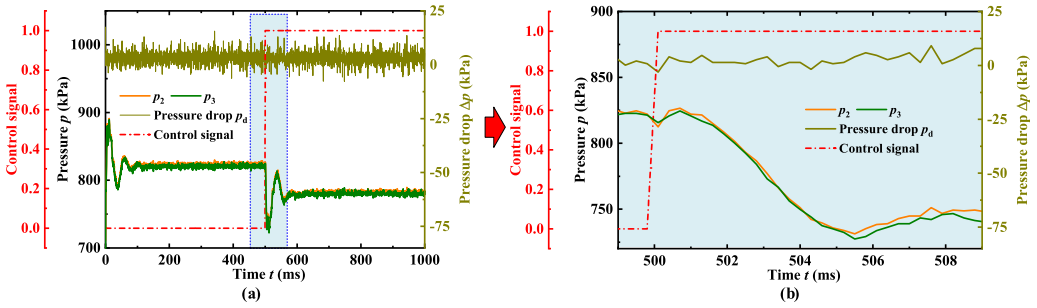

FIG. 15. The experimental results without the cantilever reed valve: (a) curves in one cycle and (b) partial magnified view of the closing process.

To confirm that the pressure variation in p_3 is induced by the CRV, an experiment is conducted in the absence of the CRV in the fixture, with the experimental findings illustrated in Fig. 15. It is clear from the results that in this condition, p_3 consistently remains approximately equal to p_2. There is no downward mutation in the pressure drop between p_2 and p_3 at 500 ms. This further proves the credibility and accuracy of selecting point A as the reference point of CRV's closing time.

3. Comparison of results between experiments and mathematical models

The back pressure is regulated by the throttle valve II to evaluate the closing time of the CRV under different operational conditions. Figure 16 presents the experimental findings. It can be seen from the figure that the CRV's closing time is 2.7 and 3.4 ms under these two operational conditions, respectively. Pressure readings, designated as p_2 and p_3, are collected through the use of pressure sensor II to indicate the CRV's inlet pressure, and pressure sensor III to indicate the outlet pressure, in succession. The pressure data p_2 and p_3 are used as input signals and put into the proposed model and the traditional model to simulate the dynamic response of the CRV. By analyzing the dynamic response, the closing time is determined, representing the duration needed for the CRV's displacement to reach zero. The results are shown in Table V.

Under different working conditions, the pressure excitation generated by the PHSV is different, which can affect the closing time of the CRV. The change rate of pressure drop is used to distinguish

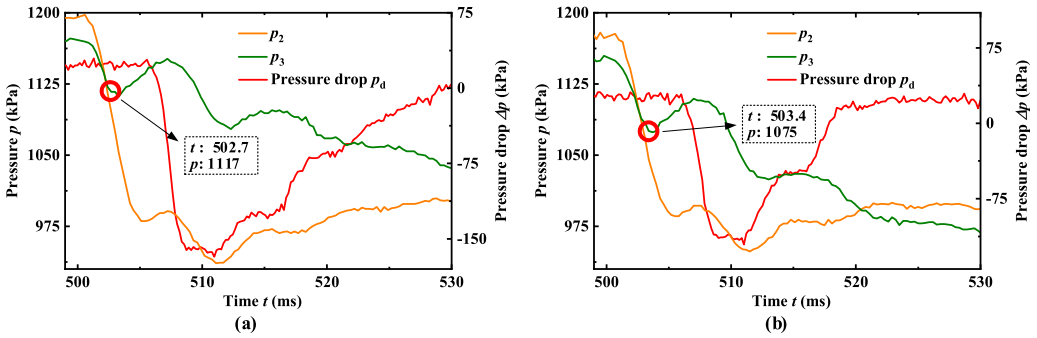

FIG. 16. (a) The experimental results under the second operational condition and (b) the experimental results under the third operational condition.

TABLE V. The comparison of results between experiments and mathematical models. The boldface is the condition in which the proposed model has the highest improvement in prediction accuracy compared with the traditional model.

Operational condition	Change rate of pressure drop (kPa/ms)	Closing time		
		Experiment (ms)	Proposed model	Traditional model
First	18	3.9	3.6 ms (7.69%)	3.3 ms (15.38%)
Second	**38**	**2.7**	**2.7 ms (0 %)**	**2.4 ms (11.11%)**
Third	22	3.4	3.1 ms (8.82%)	2.8 ms (17.65%)

different working conditions. The change rate of pressure drop is similar to the meaning of the transition time mentioned above. The calculation formula for the change rate r_p is

$$r_p = \frac{p_d(501.5) - p_d(503)}{503 - 501.5}, \tag{28}$$

where $p_d(501.5)$ and $p_d(503)$ are the pressure drop p_d at 501.5 and 503 ms, respectively.

Table V illustrates that the dynamic response of the CRV significantly improves under operational conditions that account for the transition time of pressure and back pressure. Upon analysis, it is evident that for a specified CRV, an inverse relationship exists between the closing time and the change rate of pressure drop. Under three distinct working conditions, the closing times recorded are 2.7, 3.4, and 3.9 ms, in that order. Correspondingly, the proposed model predicts closing times of 2.7, 3.1, and 3.6 ms for these conditions, while the traditional model predicts closing times of 2.4, 2.8, and 3.3 ms. Compared to the traditional model, the proposed model shows an improved prediction accuracy of 11.11%.

VI. CONCLUSION

In this paper, the influence of squeeze flow on the dynamic characteristics of CRV in the closing process is studied through finite element analysis. The squeeze force is integrated into the dynamic modeling of the CRV during closure. To verify the model's accuracy, an experimental system is constructed. Conclusions can be made as follows:

(1) The region of the CRV directly opposite the valve cover (parts A and B) experiences the squeeze force, which is related to the distance between the CRV and valve cover. A smaller distance can increase the squeeze force, thus impeding the CRV's closing motion. The region opposite the inlet (part C) is not affected by the squeeze flow and is related to the inlet pressure.
(2) The dynamic response curves of the CRV during the closing process, as predicted by the proposed model under various inlet pressures, are in close alignment with the results from the finite element analysis. In contrast, the traditional model that neglects the squeeze force yields constant predictions across diverse inlet pressures. This confirms the suitability of the proposed model for characterizing the dynamic characteristics of the CRV in place of finite element analysis.
(3) Through a comparative analysis of finite element results, the proposed model improves the prediction accuracy of fall time by reducing the maximum error from 73.26% to 18.86% when contrasted with the traditional model. Similarly, for the prediction of closing time, the proposed model decreases the maximum error from 79.29% to 23.85%.
(4) The built experimental system can independently excite the CRV. The closing time of the CRV is obtained by the inflection point of its outlet pressure. This closing time shows an inverse relationship with the change rate of pressure drop. Under actual operating conditions, the proposed model shows an enhanced prediction accuracy for closing time, surpassing the traditional model by up to 11.11%. The proposed model can be utilized for optimizing the CRV to reduce the squeeze force and enhance its dynamic characteristics in the future.

ACKNOWLEDGMENTS

This work is supported by the National Natural Science Foundation of China (Nos. 52375059 and 51975275) and the Primary Research and Development Plan of Jiangsu Province (No. BE2021034).

AUTHOR DECLARATIONS

Conflict of Interest

The authors have no conflicts to disclose.

Author Contributions

Mingming Zhang: Conceptualization (equal); Data curation (equal); Formal analysis (equal); Investigation (equal); Methodology (equal); Software (equal); Validation (equal); Visualization (equal); Writing – original draft (equal); Writing – review & editing (equal). **Yuchuan Zhu:** Conceptualization (equal); Formal analysis (equal); Funding acquisition (equal); Methodology (equal); Project administration (equal); Supervision (equal); Writing – review & editing (equal). **Linfei Li:** Formal analysis (equal); Project administration (equal); Supervision (equal); Validation (equal); Writing – review & editing (equal). **Jie Ling:** Investigation (equal); Methodology (equal); Supervision (equal); Validation (equal); Writing – review & editing (equal).

DATA AVAILABILITY

The data that support the findings of this study are available from the corresponding author upon reasonable request.

REFERENCES

[1]M. Fard, J. He, H. Huang, and Y. Cao, "Aircraft distributed electric propulsion technologies—A review," IEEE Trans. Transp. Electrif. **8**, 4067–4090 (2022).
[2]Z. Jiao, H. Zhang, Y. Shang, X. Liu, and S. Wu, "A power-by-wire aircraft brake system based on high-speed on-off valves," Aerosp. Sci. Technol. **106**, 106177 (2020).

[3]H. Li, W. Chen, Y. Feng, J. Deng, and Y. Liu, "Development of a novel high bandwidth piezo-hydraulic actuator for a miniature variable swept wing," Int. J. Mech. Sci. **240**, 107926 (2023).
[4]M. Bertin, A. Plummer, C. Bowen, N. Johnston, M. Griffiths, and D. Bickley, "A dual lane piezoelectric ring bender actuated nozzle-flapper servo valve for aero engine fuel metering," Smart Mater. Struct. **28**, 115015 (2019).
[5]H. Li, J. Liu, K. Li, and Y. Liu, "A review of recent studies on piezoelectric pumps and their applications," Mech. Syst. Signal Process. **151**, 107393 (2021).
[6]X. Wu, L. He, Y. Hou, X. Tian, and X. Zhao, "Advances in passive check valve piezoelectric pumps," Sens. Actuators, A **323**, 112647 (2021).
[7]Y. Li, V. Le, N. Goo, T. Kim, and C. Lee, "High actuation force of piezoelectric hybrid actuator with multiple piezoelectric pump design," J. Intell. Mater. Syst. Struct. **28**, 2557–2571 (2017).
[8]J. Woo, D. Sohn, and H. Ko, "Performance and flow analysis of small piezo pump," Sens. Actuators, A **301**, 111766 (2020).
[9]J. Larson and M. Dapino, "Reliable, high-frequency miniature valves for smart material electrohydraulic actuators," J. Intell. Mater. Syst. Struct. **23**, 805–813 (2012).
[10]M. Yu, S. Chen, J. Kan, Z. Zhang, C. Qian, and J. Wang, "A miniature piezo-membrane hydraulic pump with decreasing chambers in succession," J. Intell. Mater. Syst. Struct. **32**, 442–448 (2021).
[11]J. Valdovinos and G. Carman, "Development of a low-voltage piezohydraulic pump for compact hydraulic systems," Smart Mater. Struct. **24**, 125008 (2015).
[12]Z. Yang, L. Dong, M. Wang, X. Li, X. Liu, and G. Liu, "A miniature piezoelectric pump with high performance," AIP Adv. **12**, 065316 (2022).
[13]X. Yang, Y. Zhu, and Y. Zhu, "Characteristic investigations on magnetic field and fluid field of a giant magnetostrictive material-based electrohydrostatic actuator," Proc. Inst. Mech. Eng., Part G **232**, 847–860 (2017).
[14]Z. Zhang, L. He, J. Zhou, Y. Hou, D. Hu, and G. Cheng, "Design and study of an integral valve piezoelectric pump with a novel working mode," Rev. Sci. Instrum. **93**, 025006 (2022).
[15]X. Yang, "Research on magnetic field and flow field characteristic and experiment of giant magnetostrictive materials-based electro-hydrostatic actuator," Master's thesis (Nanjing University of Aeronautics and Astronautics, 2016).
[16]M. Kramer, Z. Liu, and Y. Young, "Free vibration of cantilevered composite plates in air and in water," Compos. Struct. **95**, 254–263 (2013).
[17]T. Naik, E. Longmire, and S. Mantell, "Dynamic response of a cantilever in liquid near a solid wall," Sens. Actuators, A **102**, 240–254 (2003).
[18]S. Lajimi and G. Heppler, "Comments on 'Natural frequencies of a uniform cantilever with a tip mass slender in the axial direction,'" J. Sound Vib. **331**, 2964–2968 (2012).
[19]J. Huang, J. Lou, Y. Yang, T. Chen, H. Chen, and Y. Wei, "Analysis and experiment of fluid-structure coupled vibration of MFC-actuated flexible structure immersed in viscous fluids," Chin. J. Mech. Eng. **57**, 376–385 (2021).
[20]J. Ling, L. Chen, M. Zhang, and Y. Zhu, "Development of a dual-mode electro-hydrostatic actuator with serial-parallel hybrid configured piezoelectric pumps," Smart Mater. Struct. **32**, 025011 (2023).
[21]G. Moimás, A. Abrego, D. Bueno, and J. Gasche, "Influence of the valve-seat gap on the dynamics of reed type valves," Int. J. Refrig. **118**, 238–249 (2020).
[22]J. Woo, D. Sohn, and H. Ko, "Analysis of stiffness effect on valve behavior of a reciprocating pump operated by piezoelectric elements," Micromachines **11**, 894 (2020).
[23]T. Peng, Q. Guo, J. Yang, J. Xiao, H. Wang, Y. Lou, and X. Liang, "A high flow, self-filling piezoelectric pump driven by hybrid connected multiple chambers with umbrella-shaped valves," Sens. Actuators, B **301**, 126961 (2019).
[24]Y. Wu, Z. Yang, and Y. Liu, "High frequency character of piezoelectric pump valve," Res. J. Appl. Sci., Eng. Technol. **5**, 8521–8526 (2013).
[25]J. Dong, R. Liu, W. Liu, Q. Chen, Y. Yang, Y. Wu, Z. Yang, and B. Lin, "Design of a piezoelectric pump with dual vibrators," Sens. Actuators, A **257**, 165–172 (2017).
[26]L. He, X. Wu, D. Zhao, W. Li, G. Cheng, and S. Chen, "Exploration on relationship between flow rate and sound pressure level of piezoelectric pump," Microsyst. Technol. **26**, 609–616 (2020).
[27]T. Walters, "Development of a smart material electrohydrostatic actuator considering rectification valve dynamics and in situ valve characterization," Master's thesis (School of the Ohio State University, 2008).
[28]A. Knutson and J. Van de Ven, "Modeling and experimental validation of a reed check valve for hydraulic applications," J. Dyn. Syst., Meas., Control **142**, 111001 (2020).
[29]Z. Fan, "Research on fluid-coupled piezoelectric energy harvester," Master's thesis (Harbin Institute of Technology, 2013).
[30]J. Kan, Y. Wu, Z. Yang, M. Xuan, B. Wu, and G. Cheng, "Study on the performance of micro-cantilever valve," J. Harbin Inst. Technol. **37**, 190–193 (2005).
[31]S. Chen, M. Wambsganss, and J. Jendrzejczyk, "Added mass and damping of a vibrating rod in confined viscous fluids," J. Appl. Mech. **43**, 325–329 (1976).
[32]J. Sader, "Frequency response of cantilever beams immersed in viscous fluids with applications to the atomic force microscope," J. Appl. Phys. **84**, 64–76 (1998).
[33]A. Maali, C. Hurth, R. Boisgard, C. Jai, T. Cohen-Bouhacina, and J. Aimé, "Hydrodynamics of oscillating atomic force microscopy cantilevers in viscous fluids," J. Appl. Phys. **97**, 074907 (2005).